energies

MDPI

Article

Effect of Magnetic Properties of Magnetic Composite Tapes on Motor Losses

Ryo Yoshida [1,*], Jun Kitajima [1], Takashi Sakae [1], Mitsuhide Sato [1,*], Tsutomu Mizuno [1], Yuki Shimoda [2], Akihiro Kubota [2], Shogo Wada [2], Teruo Kichiji [2] and Hideo Kumagai [2]

[1] Faculty of Engineering, Shinshu University, Nagano 380-8553, Japan
[2] TAMAGAWA Seiki Co., Ltd., Nagano 395-0068, Japan
* Correspondence: 21w2082f@shinshu-u.ac.jp (R.Y.); mitsuhide@shinshu-u.ac.jp (M.S.); Tel.: +81-26-269-5211 (M.S.)

Abstract: Alternating current (AC) copper losses in motors increase with carrier frequency of the pulse width modulation (PWM) and are further increased by leakage flux of the permanent magnet. Therefore, AC copper losses increase with motor speed. Conventional techniques for reducing AC copper losses tend to increase other losses. In this paper, AC copper loss was reduced by wrapping a magnetic tape made of a magnetic composite material around the winding. This method controlled the flux path through the winding. Magnetic composite materials are mixtures of magnetic powders and liquid resins whose magnetic properties can be manipulated by changing the combination and other factors. When Fe–Si–Al magnetic tape was wrapped around the winding, the AC copper loss was reduced by 40%. The loss was further reduced by optimizing the magnetic properties of the magnetic composite material. The AC copper loss was maximally reduced when the specific permeability was 100 and the saturation flux density was 1.6. Magnetic tapes composed of magnetic composite materials with high saturation flux density and specific permeability reduce the AC copper losses without increasing other losses in the motor.

Keywords: alternating current copper loss; drone; magnetic composite material; magnetic tape; outer rotor motor; winding

Citation: Yoshida, R.; Kitajima, J.; Sakae, T.; Sato, M.; Mizuno, T.; Shimoda, Y.; Kubota, A.; Wada, S.; Kichiji, T.; Kumagai, H. Effect of Magnetic Properties of Magnetic Composite Tapes on Motor Losses. *Energies* **2022**, *15*, 7991. https://doi.org/10.3390/en15217991

Academic Editors: João Filipe Pereira Fernandes and Silvio Vaschetto

Received: 26 September 2022
Accepted: 25 October 2022
Published: 27 October 2022

1. Introduction

In recent years, improvements in motor and inverter technologies have prompted the electrification of mobile devices [1]. The development of drone technology has been particularly remarkable. Energy can be efficiently converted by outer rotor motors with permanent magnets [2–4]. The motors used in drones and other applications must be lightweight to achieve high power density. Conventionally, motors are cooled by an air-cooling mechanism, which is lighter than water-cooling mechanisms. However, a disadvantage of air cooling is its inferior cooling capacity [5]. Therefore, a motor with low loss and low heat generation that can be sufficiently cooled by air cooling was needed. Meanwhile, the copper loss induced by carrier harmonics was reduced by applying magnetic tape to the windings. As the rotor was installed on the outside of the stator, it had a larger radius than an inner rotor and could therefore utilize a stronger inertial force, obtain a higher torque, and reach an excellent constant speed compared to the inner rotor structure. High motor speeds and torques are requirements for small-sized drones with larger payload capacities [6].

High-speed driving of a motor requires a high-speed drive frequency. A higher drive current increases the magnetic flux that contributes to torque. However, high drive frequencies and drive currents increase the motor losses caused by the chain of magnetic fluxes in the windings and cores. Structures and materials designed to reduce the iron and mechanical losses are currently being developed [7–9].

The losses generated in windings are classified into two categories: direct current (DC) copper loss and alternating current (AC) copper loss. DC copper loss is caused by current

flow through the conductor and the conductor resistance. AC copper losses (subdivided into the skin effect and proximity effect) are caused by the magnetic flux generated by AC current flow through the winding. Proximity effect refers to loss caused by the magnetic flux generated between adjacent windings. The skin effect refers to loss caused by bias of the current density inside the conductor. Current bias is induced by the magnetic flux generated by alternating current flowing in the winding. At high drive frequencies, AC copper loss is increased by sudden changes in the magnetic flux chained in the windings. Therefore, increasing the driving frequency increases both the skin and proximity effects along with the carrier frequency. It also increases magnetic flux and AC copper loss because magnetic flux leaks from the stator core chains through the windings. Therefore, reducing AC copper loss is essential, especially at speeds exceeding 10,000 rpm [10–13].

In conventional technology, the application of formed litz wire has effectively reduced AC copper loss [14,15] by reducing the cross-sectional area of the strand. Litz wire also reduces DC copper loss by improving the conductor space factor. However, litz wire is difficult to process, and therefore costly. Alternatively, the AC copper loss can be reduced by a stator with a magnetic wedge and closed-slot structure [16,17]. In this construct, a magnetic material is applied to the stator aperture to suppress slot harmonics and magnetic-resistance variations in the gap between the stator and rotor. The harmonic suppression reduces the AC copper loss and torque ripple. However, the magnetic short circuit reduces the magnetic flux, contributing to high torque. The output power of the motor, which is decreased by the torque reduction, must then be compensated by increasing the current flowing in the motor. Meanwhile, the DC copper loss generated in the windings will be proportional to the square of the current value.

Spatial harmonics can be reduced by equipping the motor stator with a magnetic composite material molded into rings or wedges [17,18]. Magnetic composite materials are synthesized by mixing a liquid resin and a magnetic powder. Magnetic composite tapes have also been developed to reduce AC copper losses in windings driven by harmonics for transformers and inductors [19,20].

As an alternative solution to the AC copper loss problem, this paper proposed a magnetic composite tape wrapped around the windings of a motor. Litz wire is used in motors because its small cross-sectional area ensures a low AC copper loss. However, its low conductor occupancy ratio tends to increase the cost of motor production. Rectangular aluminum wire has attracted attention as a low-cost material with a high conductor area fraction. However, one problem with rectangular aluminum windings is the high AC copper loss due to its flat rectangular shape [21]. Magnetic tape wrapped around the winding controls the magnetic flux path, thereby suppressing the magnetic flux chained to the winding and reducing the AC copper loss. Furthermore, by adjusting the magnetic characteristics of the magnetic tape, one could comprehensively design the tape according to the drive conditions and dimensions. Such detailed design, which would improve the efficiency of the motor, is difficult to achieve with Litz wire. Herein, the AC copper loss reduction effect of the tape was discussed. Sections 2 and 3 described the principle and analysis, respectively, of the AC copper loss reduction when the magnetic composite tape was wound around the motor winding. Section 4 described the properties of the magnetic materials for further reduction of AC copper loss.

2. Principle of Loss Reduction in Motors Attached with Magnetic Tape

2.1. Outer Rotor Motor Structure

Drones have become popular worldwide as a next-generation technology, possibly aimed at the realization of flying cars. The motor supports the drone's foundations, so its performance directly contributes to the drone's performance. In the present study, a large drone designed to carry a person on board was considered. Figure 1 shows the structure of a drone motor. This motor was an outer rotor motor with a rotor outer diameter of 179.6 mm, a rotor inner diameter of 152.4 mm, a stator inner diameter of 81.8 mm, and an axial length of 22 mm. The motor had 14 permanent magnet poles, 12 armature slots, and a

distributed winding. The permanent magnets were configured in a Halbach arrangement, which reduces the iron loss in the rotor core [22–24]. The motor was assumed to be driven at 10,000 rpm with a power output of 1 kW.

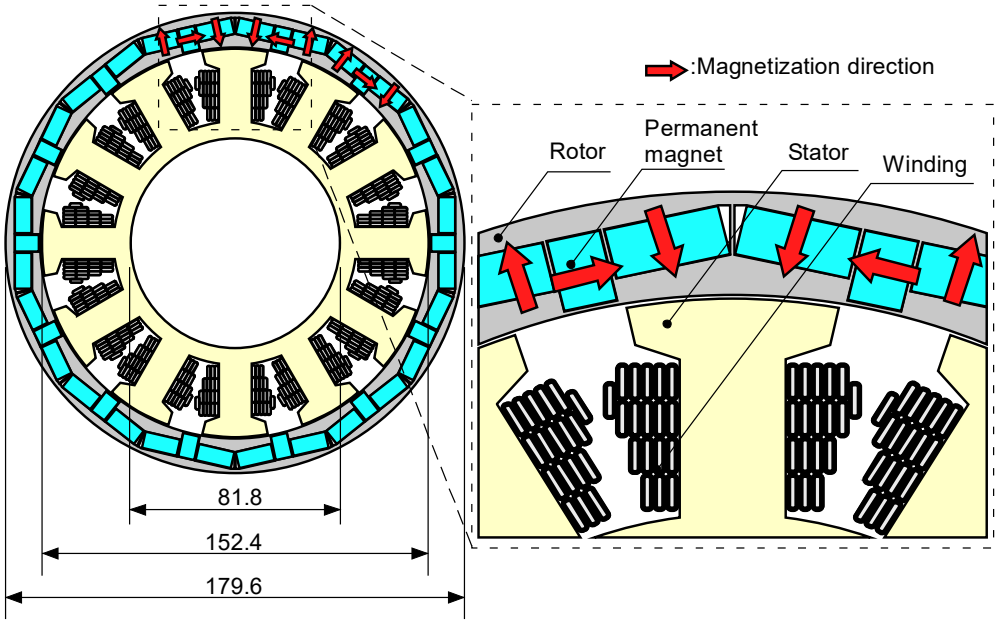

Figure 1. Structure of a drone motor (unit: mm).

2.2. Principle of AC Copper Loss Reduction in Motors

Figure 2 shows the principle by which magnetic tape controls the magnetic flux path. Figure 2a is a structural diagram of a motor without a magnetic tape winding. The magnetic flux generated by the magnets inside the rotor was chained to the teeth. As shown in Figure 2b, the windings were thinned to reduce the AC copper loss, which increased the distance between the windings. Thin wires reduced the area over which the magnetic flux chained across the windings, thereby reducing the diameter of the current at which eddy current losses could occur. However, the leakage flux of the magnetic flux chained across the teeth caused AC copper losses in the winding. Figure 2c shows the structure of a motor with magnetic tape applied to the windings. In this setup, the magnetic flux leaking from the teeth did not intersect the winding, but instead chained through the magnetic tape and returned to the teeth. The magnetic tape suppressed the magnetic flux chained to the winding, thereby reducing the AC copper loss. The magnetic layer of the magnetic tape was made of a magnetic composite material with ultra-low iron loss, so the tape generated minimal iron loss when the magnetic flux chained across the magnetic tape.

As shown in Figure 3, each winding was insulated with a 0.7-mmis thick enamel coating. Figure 3a shows the structure of the rectangular winding applied to a conventional drone motor. The increased cross-sectional area of the conductor reduced the resistance of the winding, and the DC copper loss was reduced accordingly. However, the large cross-sectional area of the conductor in the same structure induced a large AC copper loss caused by magnetic flux chain crossing. Figure 3b shows a winding structure with a thinned rectangular winding, wound with a non-magnetic tape. The thickness and width of the winding were decreased to reduce the conductor cross-sectional area—and hence the AC copper loss. In addition, the proximity effect generated in the windings was suppressed by increasing the distance between the windings [25,26]. Figure 3c shows the structure of a rectangular winding attached with magnetic tape. In addition to reducing the conductor cross-sectional area, the wrapped magnetic tape (with a specific permeability exceeding that of the winding) controlled the path of the magnetic flux chained in the winding and further reduced the AC copper loss. A 0.05-mm-thick adhesive layer was inserted between the magnetic and enamel layers of the magnetic of the magnetic tape.

The magnetic layer was made of magnetic composite material and was 0.1 mm thick. The outermost layer of the magnetic tape wrapped around the winding was a 0.055-mm-thick polyimide insulation layer.

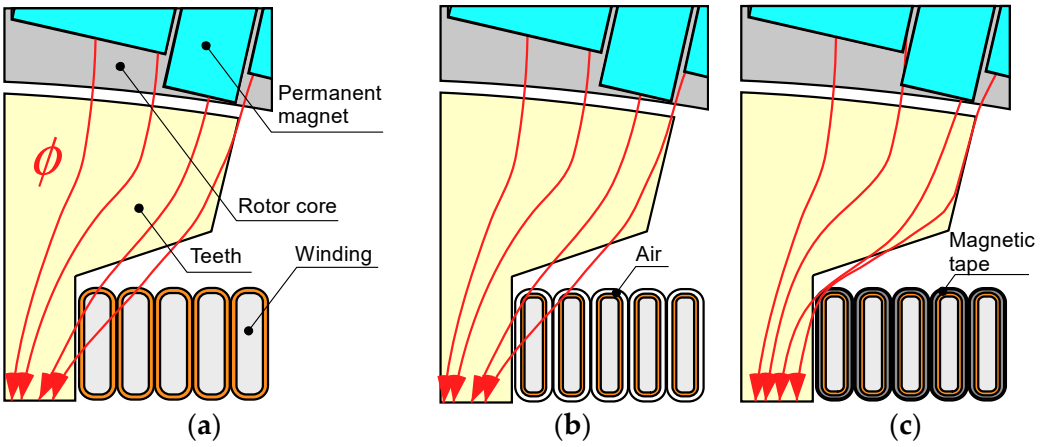

Figure 2. Magnetic flux path after installing the winding structure: (**a**) rectangular winding; (**b**) thin rectangular winding; (**c**) magnetic tape winding.

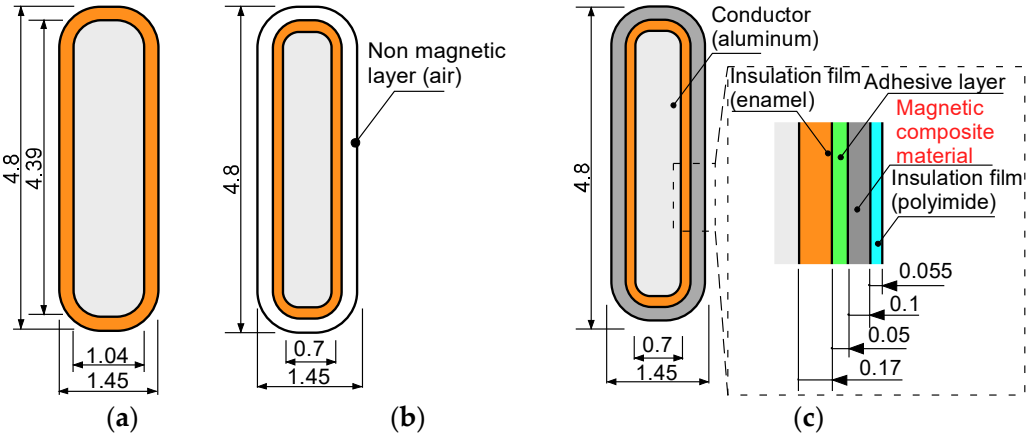

Figure 3. Winding structures (unit: mm): (**a**) rectangular winding; (**b**) thin rectangular winding; (**c**) magnetic tape winding.

Figure 4 shows the magnetic equivalent circuit of a drone motor. The magnetic flux generated from the permanent magnet inside the rotor passed through the rotor core and air gap. After being chained to the stator, it returned to the permanent magnet through the air gap and rotor core. The stator consisted of teeth, windings, a magnetic tape, and a back yoke. The magnetic flux chained to the teeth was the effective flux that contributed to torque, whereas the magnetic flux chained to the winding and magnetic tape was the leakage flux of the magnetic flux chained through the teeth. To reduce the leakage flux chained to the winding, one must increase the magnetic permeability of the magnetic tape. However, if the magnetic permeability of the magnetic tape is too large, the magnetic flux chained to the teeth decreases, thereby lowering the torque and increasing the DC copper loss. Therefore, the permeability of the magnetic tape must be larger than that of the winding and smaller than that of the electromagnetic steel plate used in the teeth. The specific permeability of magnetic composite materials (~10–100) was sufficiently smaller than that of electromagnetic steel sheets.

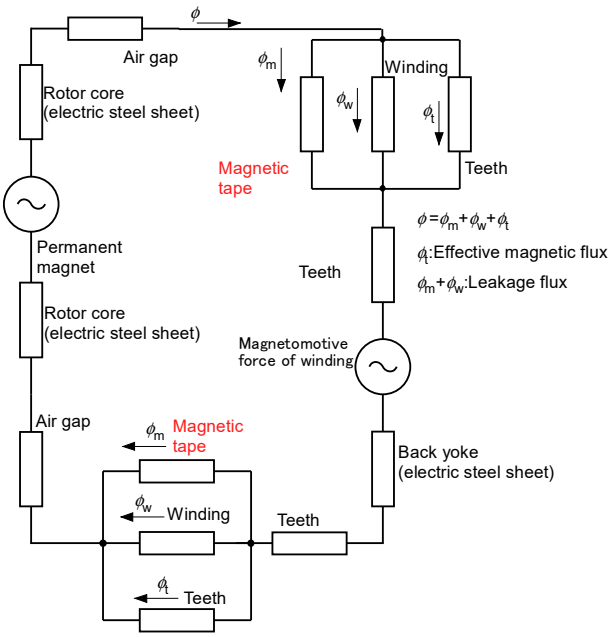

Figure 4. Magnetic circuit of the drone motor.

3. Loss Reduction Effect with Magnetic Tape

3.1. Magnetic Composite Tape

Figure 5 shows the manufacturing method of the magnetic tape formed by mixing magnetic powder with liquid resin, agitating and de-aerating the mixture, and then coating the film with a thin layer of liquid magnetic composite material using a die coater. The magnetic composite material was filled in the plunger of the die coater and poured while moving the plunger stage. Magnetic tapes were produced by thinly stretching and drying the magnetic composite materials. When mixed, the magnetic powder and liquid resin formed a low-viscosity composite which was suitable for tape-like processing. Embedding high-resistivity magnetic powder in the liquid resin reduced the path of the eddy currents generated by chaining the magnetic fluxes, thereby reducing the iron loss [27].

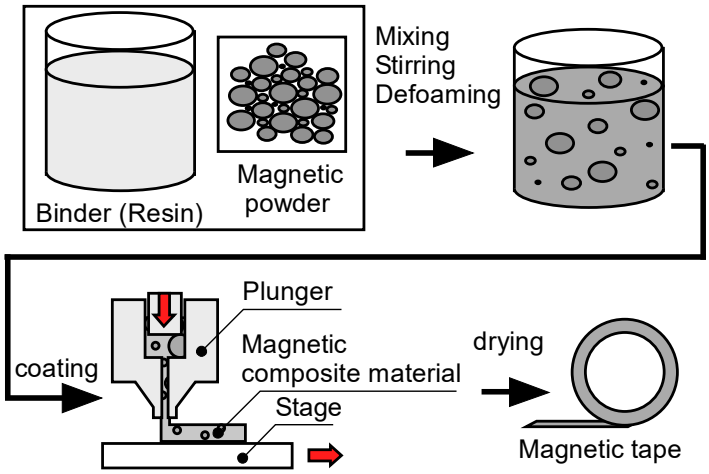

Figure 5. Manufacturing method of the magnetic tape.

Magnetic composite materials can be produced by adjusting the ratio of magnetic powder to liquid resin followed by pouring or coating and drying on sheets [28,29]. The magnetic powder in this study was Fe–Si–Al (average article diameter: 50 μm), which has low iron loss [30]. The liquid resin was epoxy resin with excellent thermosetting properties (Taiyo Wire Cloth, Duralco 4460) [31].

Panels (a) and (b) of Figure 6 show the appearance and structure of the magnetic tape, respectively. The magnetic tape was made in sheet form, cut into thin strips, and wound onto the winding wires. The thicknesses of the tape, adhesive layer, magnetic layer, adhesive layer between the magnetic layer, and insulation coating were 0.205, 0.05, 0.10, 0.03, and 0.025 mm, respectively. The magnetic tape was characterized by the magnetic composite materials in its magnetic layer. Magnetic-shielding materials reduce losses by suppressing the interaction of magnetic fluxes chained both electrically and magnetically. Therefore, the loss depends on the magnetic permeability and conductivity of the magnetic tape. Materials meeting these requirements can be formed by changing the resin material and filling ratio [31]. Although the epoxy resins used in composite materials have excellent thermal properties, they are brittle [32–34]. The brittleness problem was solved by mixing epoxy resin with magnetic power [35,36].

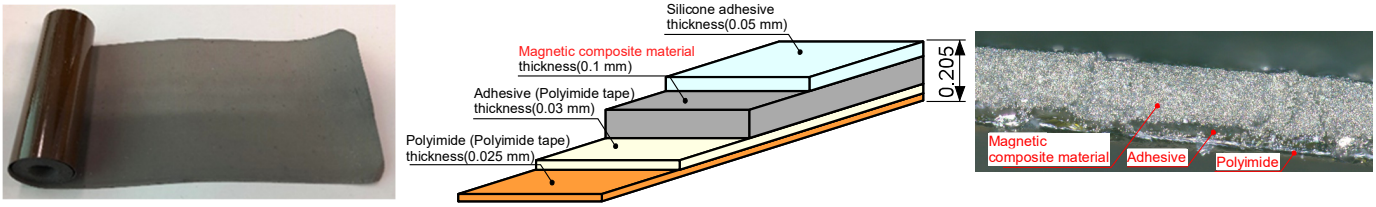

(**a**) (**b**) (**c**)

Figure 6. (**a**) Appearance and (**b**) structure of the magnetic tape (all units mm); (**c**) Digital microscope image of the magnetic tape.

The desired properties of magnetic tape can be obtained by changing the combination of materials, filling ratio, and particle size of the magnetic powder in the magnetic composite material [27]. However, if the magnetic powder filling ratio is increased to ensure high magnetic permeability, the amount of resin is necessarily reduced. Therefore, the magnetic layer is destroyed by the tensile stress generated inside the magnetic layer when the magnetic tape is wrapped around the winding. This problem can be resolved by selecting an appropriate resin and by determining the materials, structures, and manufacturing methods that best improve the degree of bonding between the powder and the resin. The polyimide outer coating has insulating properties and high heat resistance (melting temperature = 200 °C).

Figure 6c is a micrograph of the magnetic layer taken under a digital microscope (OLYMPUS, DSX-1000).

Panels (a) and (b) of Figure 7 show the magnetic properties and iron losses of the magnetic composite material, respectively. The measured samples were fabricated from Fe–Si–Al and epoxy resin as toroidal cores with an inner diameter of 20 mm, an outer diameter of 25 mm, and an axial length of 5 mm. The results were referenced to the catalog values of VACDUR 49, a material with high saturation magnetic flux density and high specific permeability provided by cobalt. VACDUR 49 is used in rotor and stator cores and its saturation magnetic flux density is 2.3 T, versus 0.7 T in the Fe–Si–Al magnetic composite. The maximum permeability of the magnetic composite material was less than one-hundredth that of VACODUR 49. Meanwhile, the iron loss of the magnetic composite material (Figure 7b) was measured at an excitation frequency of 1 kHz using a magnetic flux/magnetic-field-strength (B–H) analyzer (Iwatsu, SY-8218, province, country). Again, the catalog iron loss values of VACODUR 49 were referenced for comparison. The iron loss of the magnetic composite material was difficult to measure above 0.4 T, owing to the current capacity limitation of the bipolar amplifier of the B–H analyzer. Therefore, the B–H curve in the region below 0.4 T was approximated from the measured data using the experimental formula for iron loss $P_{i:}$

$$P_i = K_h f B_m{}^{1.6} + K_e f B_m \ (\mathrm{W/m^3}). \quad (1)$$

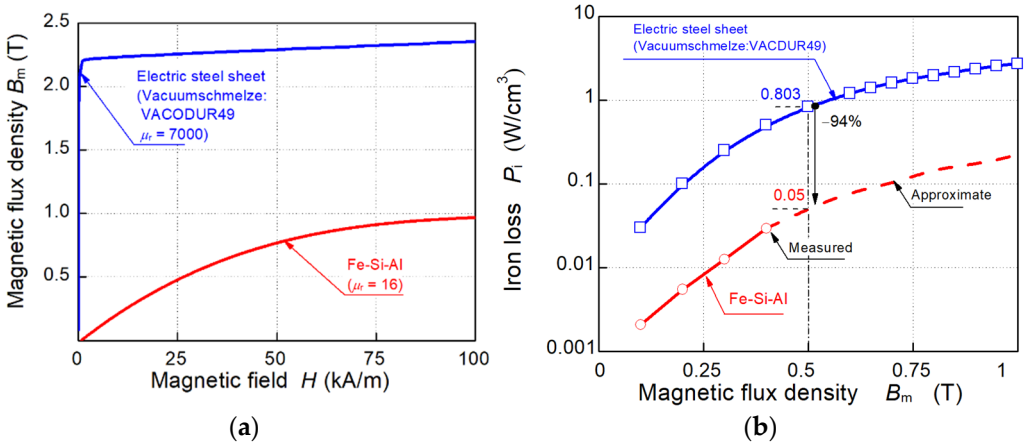

Figure 7. Magnetic characteristic of magnetic composite material (**a**) DC magnetic characters; (**b**) iron loss characteristics.

Here, K_h is the hysteresis loss coefficient (J/(T$^{1.6}$m^3)), f is the frequency (Hz), B_m is the maximum magnetic flux density (T), and K_e is the eddy current loss coefficient (m/Ω).

3.2. Analysis of a Motor with Magnetic Tape-Wrapped Windings

Next, the characteristics of a motor with rectangular windings, a motor with finer rectangular windings, and motors with magnetic tape-wrapped windings were examined under the conditions given in Table 1. Each analysis was performed twice: once with the current superimposed on the carrier harmonics assuming an inverter, and once with the current at the fundamental wavelength only. The analysis method was a two-dimensional electromagnetic-field transient-response analysis implemented in JMAG Designer software (ver. 19.1). The mesh of the winding was set sufficiently small to account for skin effects. The output power was 10 kW, the speed was 10,000 rpm, and the synchronous frequency was 1166 Hz. To analyze the effect of carrier harmonics, the ripple factor was increased from 10% to 100% at 40 kHz. The current was set to gain the same torque for each motor. The electromagnetic steel plates of the stator of the conventional motor were constructed from permendur alloy with a high saturation flux density. The magnetic composite material was used as the magnetic layer of the magnetic tape.

Table 1. Analysis conditions.

Item	Contents	
Software	JMAG Designer (64) Ver.19.1	
Analysis method	Two-dimensional transient-response magnetic field analysis	
Solution	FEM	
Mesh size	(1) magnetic tape: Auto (2) Copper: 0.1 mm (1/8 of the skin effect) (3) Teeth: Auto (4) Permanent magnet: 0.2 mm (5) Air: Auto	
Analysis area	Analysis in 5 times the analysis model	
Rotate speed	10,000 rpm	
Frequency	1166 Hz	
Torque	9.95 Nm	
Carrier frequency	none	40 kHz
Current	Rectangular winding: 13.4 A	13.4 A (ripple 10–100%)
	Thin rectangular winding 13.5 A	-
	Magnetic tape winding 13.4 A	13.3 A (ripple 10–100%)

Table 1. *Cont.*

Item	Contents
Materials	(1) Aluminum: ($\rho = 2.92 \times 10^{-8}$ Ωm, $\mu' = 1$, $\mu'' = 0$) (2) Permanent magnetLHitachi material: NMX41-EH) (3) Rotor core: (Vacuumschmelze: Permendur VACODUR49) (4) Stator core: (Vacuumschmelze: Permendur VACODUR49) (5) Magnetic tape: Magnetic composite material (6) Air: ($\mu = \infty$ Ωm, $\mu' = 1$, $\mu'' = 0$)

Figure 8 shows a current waveform with a fundamental frequency of 1166 Hz superimposed with 20% of the 40-kHz as carrier harmonic. Consequently, the inverter assumed to drive the motor exhibited a 20% ripple factor in its waveform.

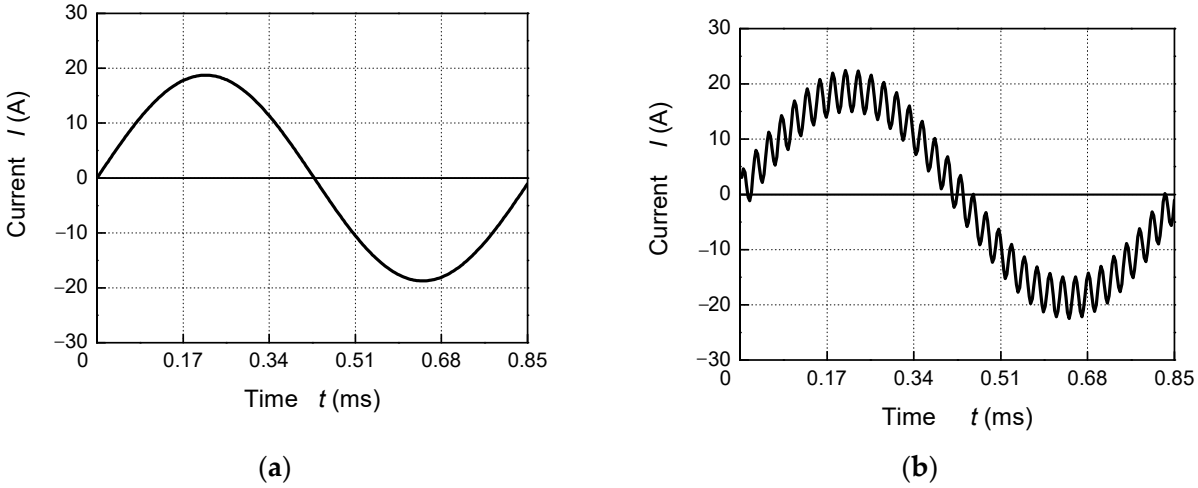

Figure 8. Current waveform superimposed with carrier harmonics: (**a**) ripple = 0%; (**b**) ripple = 20%.

Panels (a) and (b) of Figure 9 show the distributions of magnetic flux density in the motors with bare and magnetic tape-wrapped rectangular windings, respectively. Unlike the magnetic flux density in the bare winding, the magnetic flux density of the winding with magnetic tape was suppressed to 0.5 T owing to induced leakage flux.

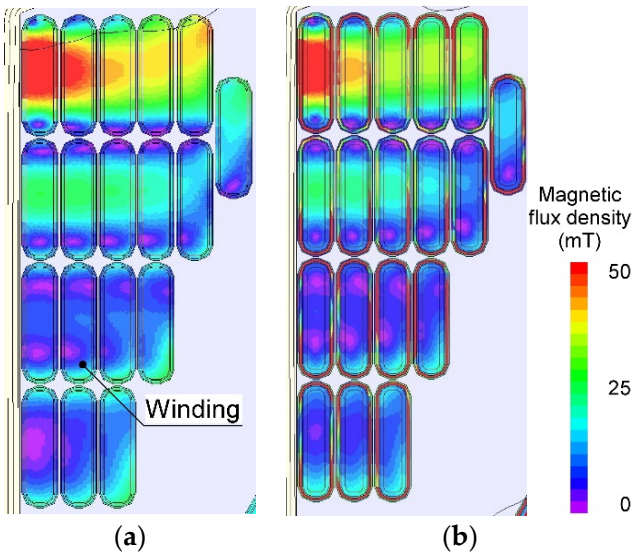

Figure 9. Distributions of magnetic flux density in the (P_o = 10 kW, N_r = 10,000 rpm, θ_e = 69°) (**a**) rectangular winding; (**b**) magnetic tape-wrapped winding.

Panels (a) and (b) of Figure 10 show the current density distributions in the motors with bare and magnetic tape-wrapped rectangular windings, respectively. The magnetic tape reduced the current density from that of the bare winding. The DC copper loss of a motor with windings was reduced by the enlarged conductor area; however, when the windings were wrapped with magnetic tape, the AC copper loss was reduced by the decreased conductor cross-sectional area of the windings and the increased distance between the windings. The leakage flux was then chained to the magnetic tape rather than to the windings.

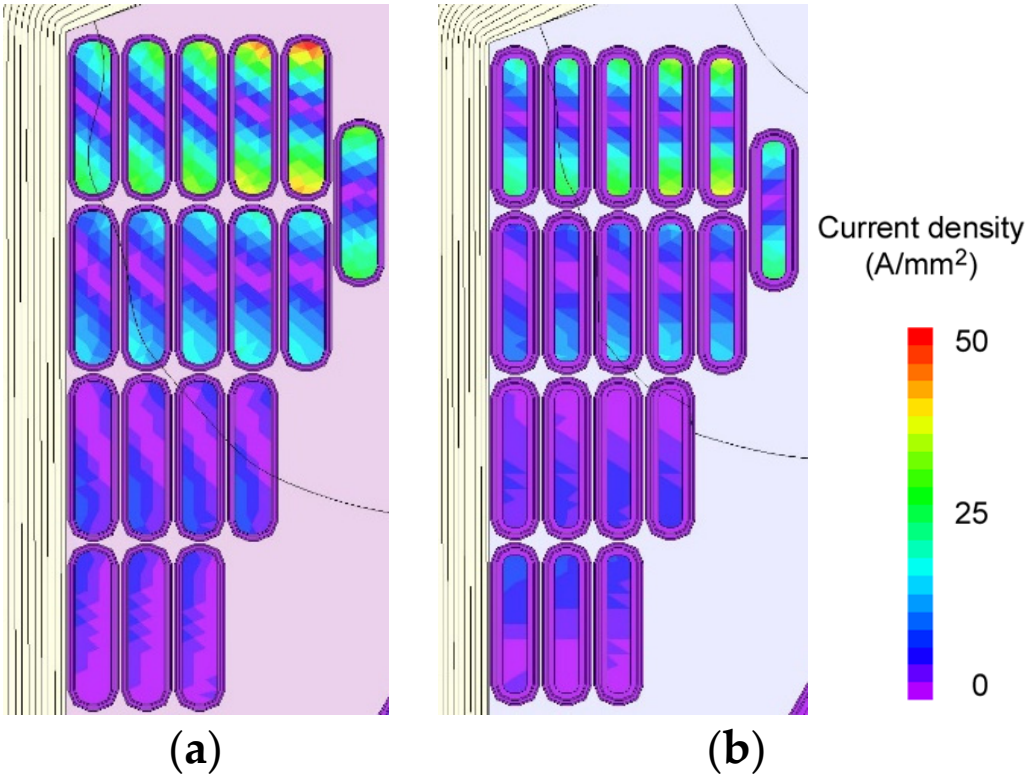

Figure 10. Distributions of current density. (P_o = 10 kW, N_r = 10,000 rpm, θ_e = 69°) (**a**) rectangular winding; (**b**) magnetic tape-wrapped winding.

Figure 11 shows the loss characteristics of the motors running at 10,000 rpm with an output of 10 kW. The PWM frequency of the inverter was a harmonic that increased the motor losses during the drive. Therefore, we confirmed the effect of reducing the loss generated by harmonics under actual driving conditions. The losses of the motors with rectangular windings, fine rectangular windings, and magnetic tape-wrapped rectangular windings were 791, 766, and 758 W, respectively, and the efficiencies were 92.1%, 92.3%, and 92.4%, respectively. The losses were lowest in the motor with magnetic tape-wound square wires. The flat-wire motor, fine flat-wire motor, and flat-wire-motor with magnetic tape exhibited copper losses of 112, 77, and 73 W, respectively, and AC copper losses of 97, 62, and 58 W, respectively. The AC copper loss was 37 W lower in the motor with magnetic tape than in the motor with bare winding. Further loss reduction can be expected by increasing the specific permeability and saturation flux density of the magnetic tape. Although the 20% ripple assumed in actual driving increased the motor losses, this increase was more than offset by the loss reduction effect of the magnetic tape winding.

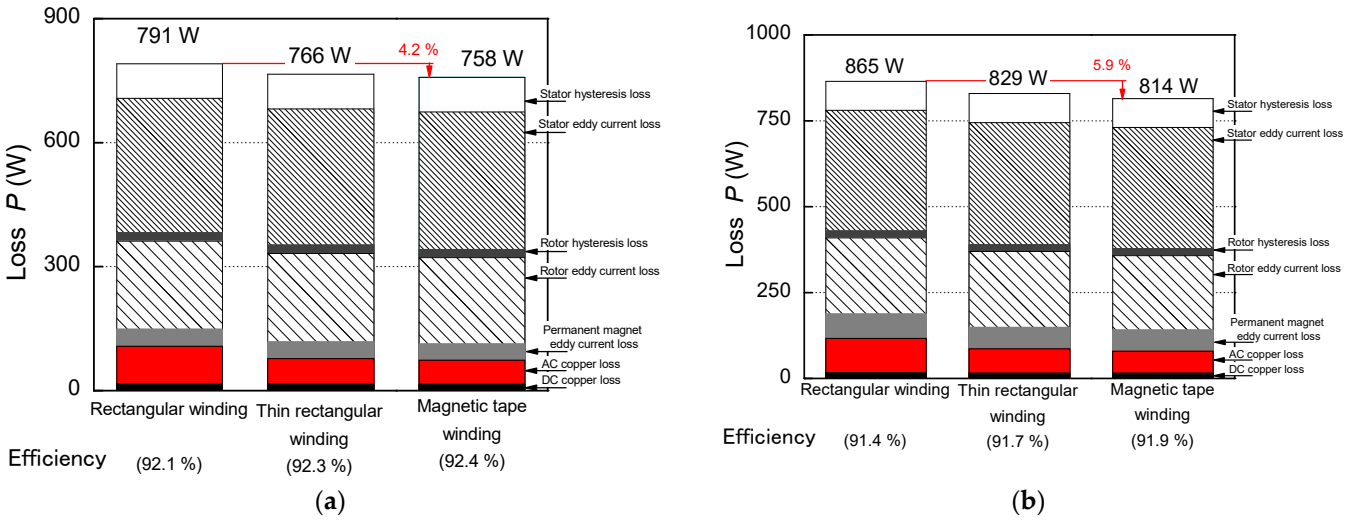

Figure 11. Loss characteristics of the motors (P_o = 10 kW, N_r = 10,000 rpm): (**a**) fundamental; (**b**) 20% ripple.

4. Magnetic Properties of Magnetic Tape for Improving the AC Copper Loss Reduction

4.1. Effect of Magnetic Properties of Materials on Motor Losses

To improve the AC copper loss-reduction effect, the specific permeability and saturation magnetic flux density of the magnetic composite material were varied as parameters. Figure 12 shows the DC magnetization characteristics of hypothetical materials with various saturation magnetic flux densities (0.8, 1.0, 1.2, 1.4, and 1.6 T), and specific permeabilities (20, 50, 75, and 100): a total of 20 conditions.

The selected saturation flux densities and specific permeabilities were those expected for magnetic composite materials with different material types and shapes.

Figure 13 shows the AC copper losses in the motor as the magnetic properties of the magnetic tape were changed. The higher the specific permeability and saturation magnetic flux density, the smaller the AC copper loss. Within the practical range of magnetic composite materials, the AC copper loss was minimized at 14 W when the specific permeability and saturation magnetic flux density were 100 and 1.6 T, respectively. The larger the specific permeability and saturation magnetic flux, the more effective the reduction of AC copper loss. The loss generated by the magnetic tape (of the order of 10^{-1}) was almost negligible. At specific permeabilities around 20, the AC copper loss reduction effect was suppressed even at a saturation magnetic flux density of 1.6 T because the magnetic flux path was not fully controlled. Meanwhile, at saturation magnetic flux densities around 0.8 T, the AC copper loss increased even at a specific permeability of 100 because magnetic flux leaked from the magnetic tape and crossed the winding. When the specific permeability was changed, the largest difference in AC copper loss was 5.21 W at a saturation magnetic flux density of 1.6 T. When the saturation magnetic flux density was changed, the largest difference in AC copper loss was 3.32 W at a specific permeability of 100.

Figure 14 compares the losses in motors with different types of magnetic tapes: the Fe–Si–Al magnetic tape and a magnetic tape made of ideal magnetic composite material. The AC copper losses of the motors with the Fe–Si–Al magnetic tape and ideal magnetic material were 58 and 14 W, respectively. Applying the magnetic tape made of ideal magnetic material reduced the AC copper loss by 76%, thereby improving the motor efficiency by 0.35%. Owing to its high specific permeability and saturation flux density, this material controlled the magnetic flux path by chaining the magnetic flux to the magnetic tape rather than to the winding.

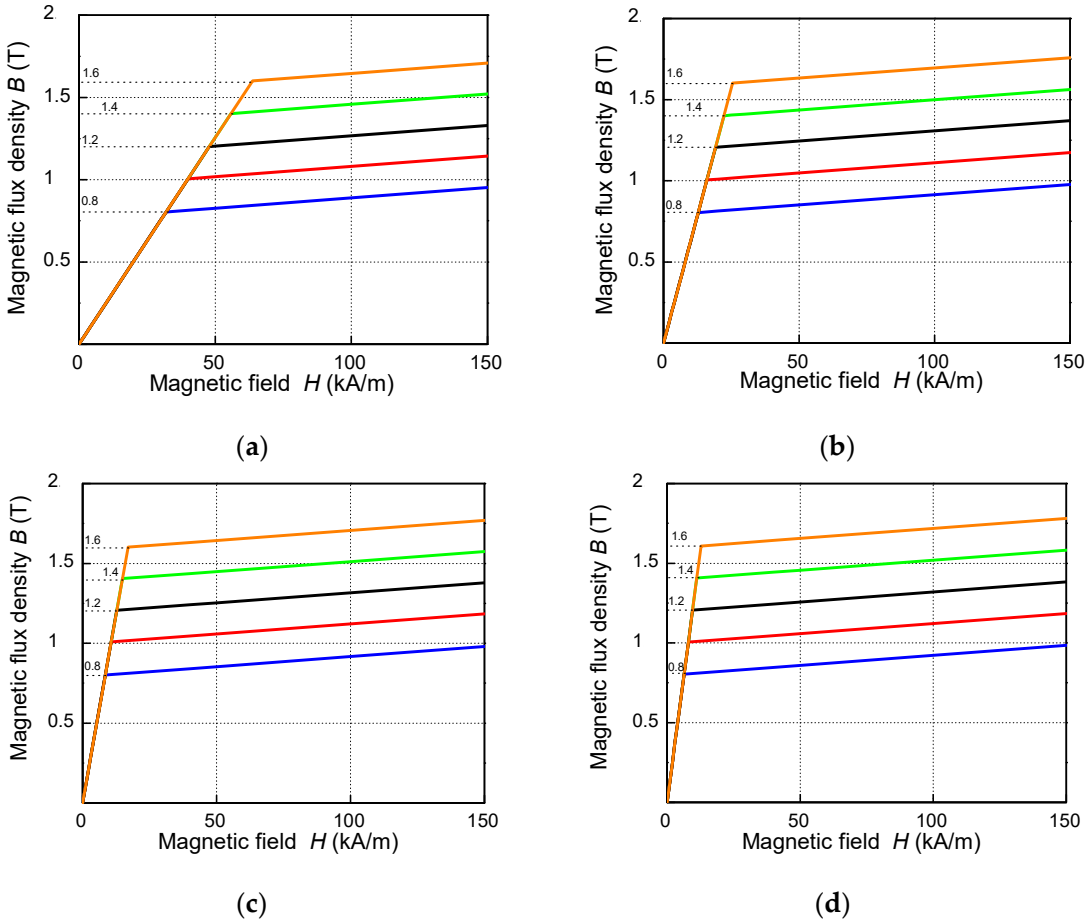

Figure 12. Magnetic properties of hypothetical magnetic tapes with different specific permeabilities ((**a**) μ_r = 20; (**b**) μ_r = 50; (**c**) μ_r = 75; (**d**) μ_r = 100) and magnetic flux densities: 0.8 (blue), 1.0 (red), 1.2 (black), 1.4 (green), and 1.6 T (orange).

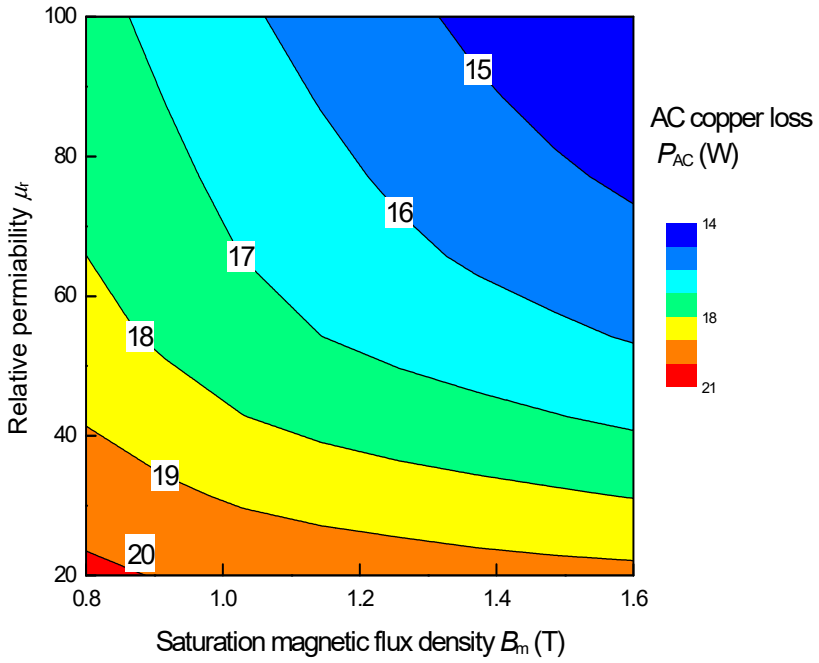

Figure 13. Distribution of AC copper loss in motors with hypothetical materials.

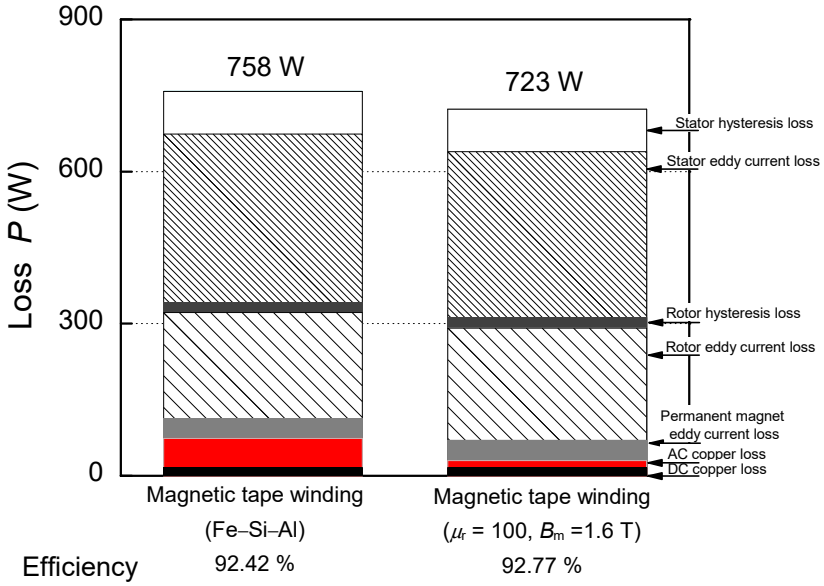

Figure 14. Loss comparison of motors with windings wrapped with (**left**) Fe–Si–Al magnetic tape and (**right**) a magnetic tape made of ideal magnetic composite material (P_o = 10 kW, N_r = 10,000 rpm).

Figure 15 shows the torque–current characteristics of the motors running at 10,000 rpm. The torque constants of the motors with the Fe–Si–Al magnetic tape and the ideal magnetic tape were 0.71 and 0.72 Nm/A, respectively. As the torque constant was almost unchanged by altering the magnetic permeability and saturation flux density of the magnetic tape, the DC copper loss was unchanged and only the AC copper loss was reduced.

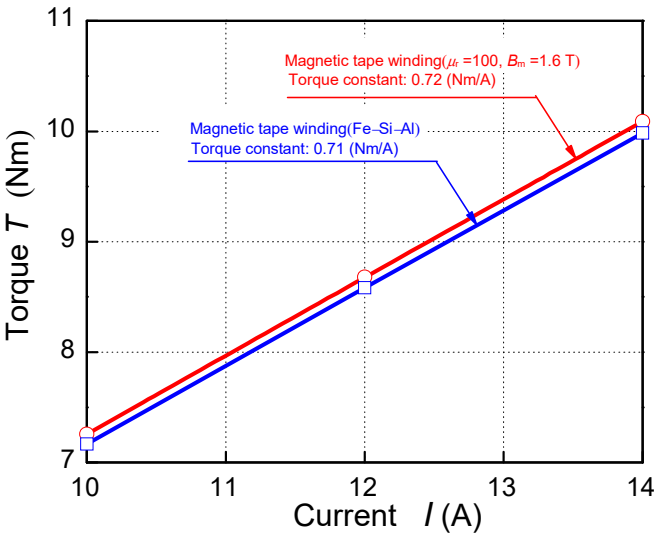

Figure 15. Torque–current characteristics of the motors described in Figure 14 (N_r = 10,000 rpm).

Panels (a), (b), and (c) of Figure 16 compare the motor efficiencies, copper losses, and iron losses, respectively, as functions of ripple rate of the carrier harmonic (40 kHz). The efficiencies of both motor types decreased as the ripple factor increased from 0% to 100%. In the 10% to 50% region of ripple factors, the efficiency of the virtual tape-wrapped motor. At ripple rates above 50%, the efficiency of the Fe–Si–Al tape winding motor exceeded that of the ideal magnetic tape winding motor.

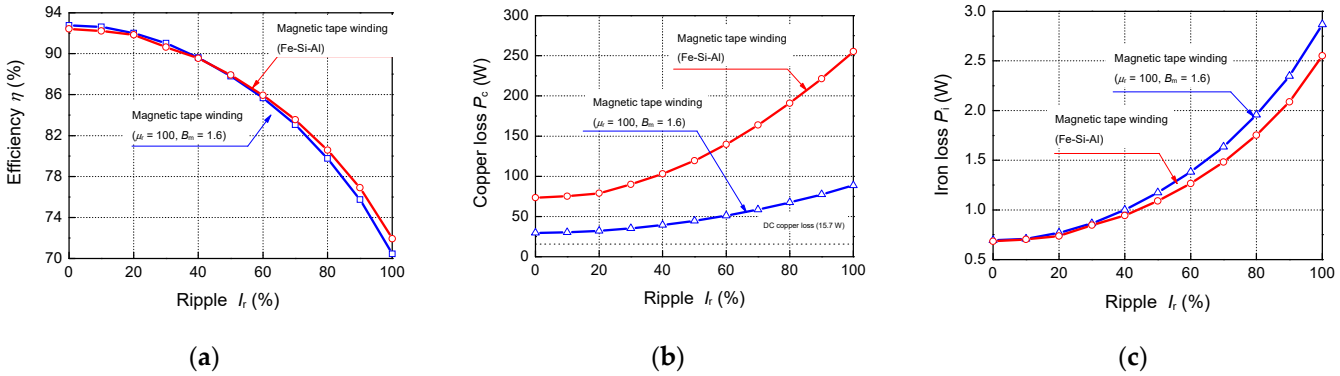

Figure 16. Comparison of tape-dependent motors losses (P_o = 10 kW, N_r = 10,000 rpm). (**a**) efficiency; (**b**) copper loss; (**c**) iron loss.

The DC copper loss was 15.7 W for both motor types. In both cases, the AC copper loss was higher with a ripple factor of 100% than with a ripple factor of 10%. The virtual tape better suppressed the increase in copper loss than the Fe–Si–Al tape because its high specific permeability and saturation flux density strongly attracted leakage flux. The iron loss of the Fe–Si–Al tape-wrapped motor was small at all ripple rates, but it increased as the ripple rate increased.

4.2. Effect of Carrier Harmonics on Motor Losses

Panels (a) and (b) of Figure 17 show the distribution of magnetic flux density in the Fe–Si–Al tape-wound motor and a virtual material tape-wound motor. The higher specific permeability of the virtual material (compared to the Fe–Si–Al tape) induced leakage flux in the teeth; consequently, the magnetic flux density was higher in the teeth of the virtual material tape-wound motor than in the teeth of the Fe–Si–Al tape-wound motor. The higher flux density in the teeth slightly increased the torque of the motor. The torques of the Fe–Si–Al tape-wound motor and the virtual material tape-wound motor were 9.37 and 9.41 Nm, respectively.

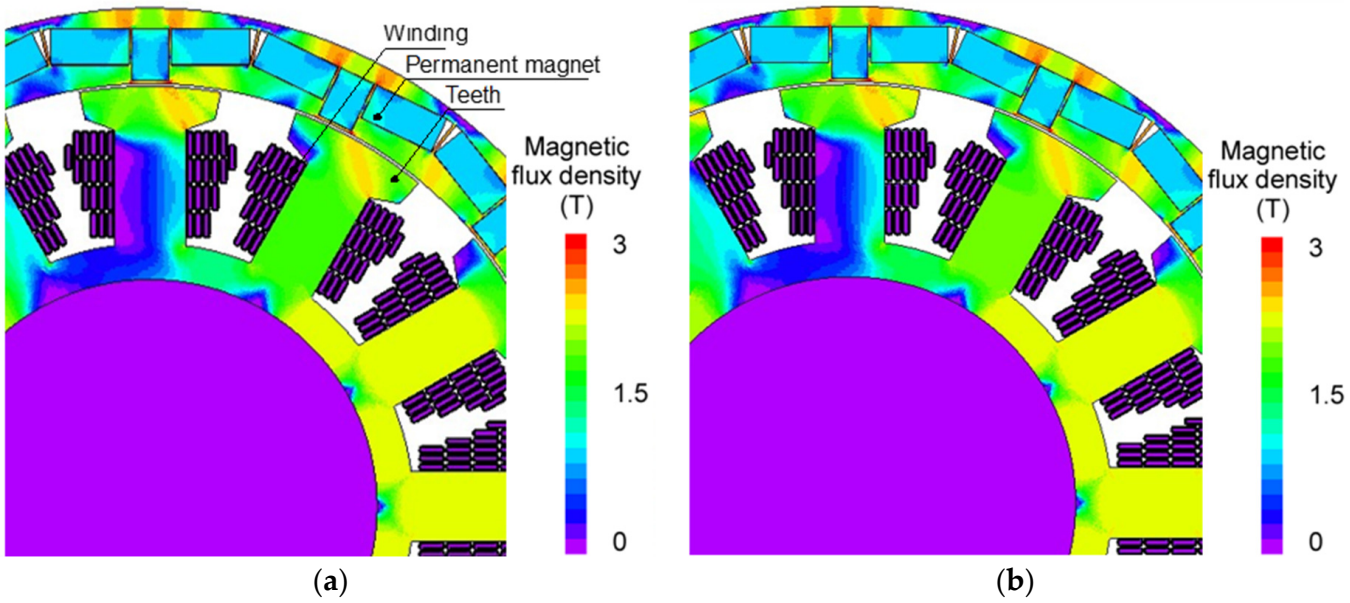

Figure 17. Magnetic flux density distribution in the motors (P_o = 10 kW, N_r = 10,000 rpm) (**a**) Fe–Si–Al tape windings; (**b**) virtual tape windings.

Table 2 compares the contour plots of iron loss distributions in the motors with Fe–Si–Al tape windings and virtual tape windings at the fundamental frequency (1166 Hz) and

the 40-kHz carrier harmonic. Here, the Fe–Si–Al tape windings were compared against the virtual material with a specific permeability of 100 and a saturation magnetic flux density of 1.6 T, which achieved the best copper loss reduction. The iron loss due to the fundamental frequency was almost independent of specific permeability and saturation magnetic flux density of the magnetic tape, but the iron loss due to carrier harmonics (40 kHz) was higher in the virtual tape-wound motor than in the Fe–Si–Al tape-wound motor. A magnetic tape with high permeability induced leakage flux into the teeth, increasing the iron loss. When the ripple ratio exceeded 50%, the iron loss in the teeth of the motor with the virtual tape dominated the AC copper loss reduction effect, so the efficiency declined from that of the Fe–Si–Al tapes. Reducing copper loss is essential for suppressing heat generation in drone motors. The AC copper losses can be reduced by employing magnetic composite materials with high specific permeability and saturated magnetic flux density. The reduction effect is particularly significant at high speeds (>10,000 rpm). However, when considering the carrier harmonics during actual driving, materials with high specific permeability increase the iron loss generated in the teeth. The efficiencies of the real materials were less than the losses in virtual materials with ripple ratio of carrier harmonics greater than 40%. Therefore, the magnetic characteristics of a designed magnetic tape should account not only for the frequency of carrier harmonics, but also for the ripple factor.

Table 2. Iron loss distributions at different frequencies (P_o = 10 kW, N_r = 10,000 rpm, ripple = 100%).

Tape	Frequency	
	1166 Hz (fundamental frequency)	40 kHz (harmonic frequency)
Fe–Si–Al	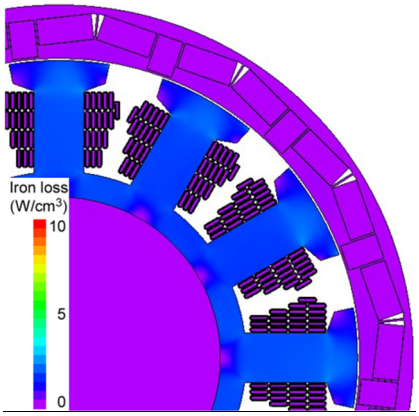	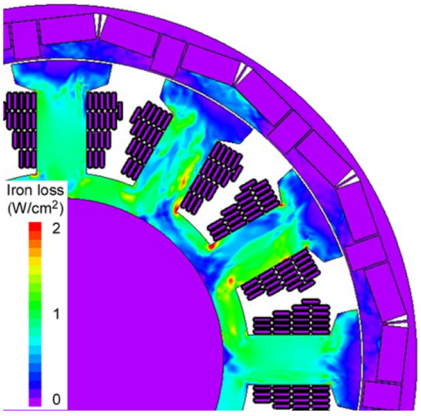
μ_r = 100, B_m = 1.6 (Virtual)	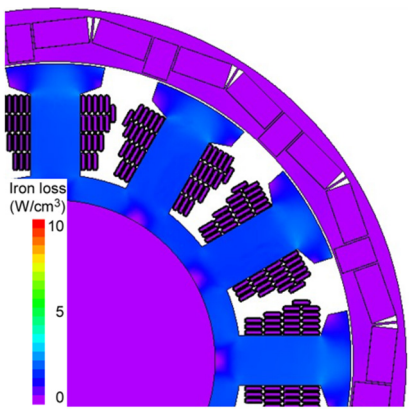	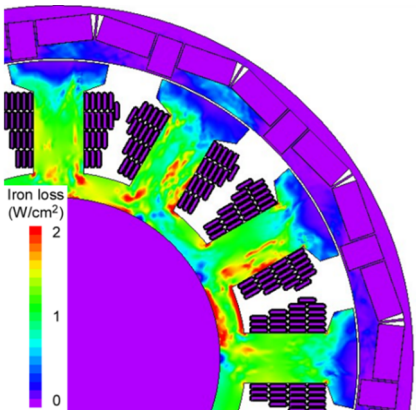

5. Conclusions

In this paper, magnetic tape constructed from a magnetic composite material was applied to the windings of drone motors to reduce their AC copper loss.

The magnetic composite material was synthesized by mixing a magnetic powder and liquid resin. It could be formed into a tape or cast as a slurry. The desired magnetic properties were obtained by changing the material of the resin, the particle size and shape of the metal powder, and the filling ratio of the material.

An aluminum-wound motor with an outer rotor was assumed to operate at high power density in drones. When magnetic tape was applied to the windings of a motor running at 10,000 rpm with a power output of 10 kW, the AC copper loss was reduced by 40%.

The influences of the magnetic properties of the magnetic tapes on the motor losses were investigated. Increasing the specific permeability and saturation flux density of the magnetic tape enhanced the reduction of AC copper loss in the motor. Simulations confirmed that the virtual magnetic properties of magnetic composites influenced AC copper loss reduction. The AC copper loss was maximally reduced when the magnetic permeability was 100 and the saturation magnetic flux density was 1.6 T. The DC copper loss was unaffected by applying magnetic tape to the winding.

At higher carrier harmonics, the magnetic tape with high specific permeability increased the magnetic flux density in the teeth, inducing leakage flux into the teeth and consequent iron loss. Therefore, to improve the motor efficiency, the selected magnetic tape should suppress not only the copper loss, but also the iron loss due to carrier harmonics.

Author Contributions: Conceptualization and methodology, R.Y., M.S. and T.M.; software, J.K. and T.S.; writing—review and editing, project administration, funding acquisition, Y.S., A.K., S.W., T.K. and H.K. All authors have read and agreed to the published version of the manuscript.

Funding: This research was funded by New Energy and Industrial Technology Development Organization (NEDO), grant number P15005.

Data Availability Statement: The data presented in this study are available on request from the corresponding author. The data are not publicly available due to the large amount of data.

Conflicts of Interest: The authors declare no conflict of interest.

References

1. Kwok, C.T.; Ching, C.C.; Chunhua, L. Overview of permanent-magnet brushless drives for electric and hybrid electric vehicles. *IEEE Trans. Ind. Electron* **2018**, *55*, 2246–2257.
2. Chan, K.W.; Nirmal, U.; Cheaw, W.G. Progress on Drone Technology and Their Applications: A Comprehensive Review. *AIP Conf. Proc.* **2018**, *2030*, 020308.
3. Tumbek, M.; Kesler, S. Design and Implementation of a Low Power Outer-Rotor Line-Start Permanent-Magnet Synchronous Motor for Ultra-Light Electric Vehicles. *Energies* **2019**, *12*, 3174. [CrossRef]
4. Yuan, Y.; Wenjun, M.; Xiaoxia, S.; Liyong, Z. Design Optimization and Analysis of an Outer-Rotor Direct-Drive Permanent-Magnet for Medium-Speed Electric Vehicle. *World Electr. Veh. J.* **2019**, *10*, 16. [CrossRef]
5. Bae, J.C.; Cho, H.R.; Yadav, S.; Kim, S.C. Cooling Effect of Water Channel with Vortex Generators on In-Wheel Driving Motors in Electric Vehicles. *Energies* **2022**, *15*, 722. [CrossRef]
6. Henke, M.; Narjes, G.; Hoffman, J.; Wohlers, C.; Urbanek, S.; Heister, C.; Steinbrink, J.; Caanders, W.; Ponick, B. Challenges and Opportunities of Very Light High-Performance Electric Drives for Aviation. *Energies* **2018**, *11*, 344. [CrossRef]
7. Sai, B.; Tawhid, T.M.B.; Seungdeog, C. Optimal Torque Ripple Reduction Technique for Outer Rotor Permanent Magnet Synchronous Reluctance Motors. *IEEE Trans. Energy Convers.* **2018**, *33*, 1184–1192.
8. Liyi, L.; Jiangpeng, Z.; Chengming, Z.; Jikun, Y. Research on Electric and Thermal Issue of High-Efficiency and High-Power-Density Outer-Rotor Motor. *IEEE Trans. Appl. Superconuctivity* **2016**, *26*, 5204805. [CrossRef]
9. Andrqej, L. Design, Analysis of the Location and Materials of Neodymium Magnets on the Torque and Power of In-Wheel External Rotor PMSM for Electric Vehicles. *Energies* **2018**, *11*, 2293.
10. Iwasaki, I.S.; Rajesh, D.P.; Yong, L.; Adam, P.; Zhu, Z.Q.; Bremner, J.J. Influence of PWM on the Proximity Loss in Permanent-Magnet Brushless AC Machines. *IEEE Trans. Ind. Appl.* **2009**, *45*, 4. [CrossRef]
11. Woo, J.; Bang, T.; Lee, J.; Lee, H.; Choi, J. Experimental Verification and Analytical Approach for Electromagnetic Characteristics of a High-Speed Permanent Magnet Motor with Two Different Rotors and Winding Patterns. *Appl. Sci.* **2021**, *11*, 9060. [CrossRef]
12. Aitakkache, M.; Enrici, P.; Matt, D.; Boudaker, N.; Piscini, L. Concept, Feasibility of Cylindrical Bar Winding for Low Voltage Permanent Magnet Synchronous Motor. *Energies* **2022**, *15*, 1507. [CrossRef]
13. Juha, P.; Tapani, J.; Valeria, H. *Design of Rotating Electrical Machines*; John Wiley & Sons: Hoboken, NJ, USA, 2013.

14. Andreas, R.; Carla, B. Enhancing Litz Wire Power Loss Calculations by Combining a Sparse Strand Element Equivalent Circuit Method with a Voronoi-Based Geometry Model. *IEEE Trans. Power Electron.* **2022**, *37*, 9.
15. Dimier, T.; Cossale, M.; Wellerdicck, T. Comparison of Stator Winding Technologies for High-Speed Motors in Electric Propulsion Systems. In Proceedings of the 2020 International Conference on Electrical Machines (ICEM), Gothenburg, Sweden, 23–26 August 2020; pp. 2406–2412.
16. Han, Y.; Chen, S.; Gao, C.; Gao, M.; Si, J.; Hu, Y. Effect of Slot Opening Width on the Air-Gap magnetic Field of a Direct Drive Permanent Magnet Motor. *Appl. Sci.* **2019**, *9*, 4649. [CrossRef]
17. Manabu, H.; Ryoken, M.; Mitsuhide, S.; Yiggen, B.; Masami, N.; Tsutotmu, M. Reduction of Rotor Loss and Torque Ripple in an IPMSM using Magnetic Wedge. In Proceedings of the IEEE 2020 23rd International Conference on Electrical Machines and Systems (ICEMS), Hamamatsu, Japan, 24–27 November 2020; pp. 498–503.
18. Mitsuhide, S.; Keigo, T.; Manabu, H.; Ryoken, M.; Ryo, Y.; Masami, N.; Yeggin, B.; Tsutomu, M. Reducing Rotor Temperature Rise in Concentrated Winding by Using Magnetic Power Mixed Resin Ring. *Energies* **2020**, *13*, 6721.
19. Kazuhiro, S.; Kazuma, K.; Mitsuhide, S.; Tsutomu, M.; Norio, K.; Masayuki, S.; Takao, N. Alternating-Current Copper Loss Reduction in a High-frequency Transformer for Railways Using Magnetic Tape. *IEEE Trans. Magn.* **2021**, *57*, 2021.
20. Mitsuhide, S.; Kaito, S.; Kazuma, K.; Syun, E.; Tsutotmu, M. Reducing the Alternating Current Resistance and Heat Generation in a Single-Wire Coil Using a Magnetic Tape. *IEEJ Trans. Electr. Electr. Eng.* **2020**, *15*, 1541–1548.
21. Pil, H.W.; Yon, C.D.; Jae, C.H.; Mi, K.J.; Dae, K.H.; Ju, L. The study to substitute aluminum for copper as a winding material in induction machine. In Proceedings of the INTELEC 2009 31st International Telecommunications Energy Conference, Incheon, Korea, 18–22 October 2009. [CrossRef]
22. Cacurar, P.; Vasile, T.; Adina, G.; Calin, M.; Claudia, C.; Sergiu, A.; Marian, G. Modelling and Analysis of the Halbach Array Magnets. In Proceedings of the 2019 11th International Symposium on Advanced Topics in Electrical Engineering (ATEE), Bucharest, Romania, 28–30 March 2019. [CrossRef]
23. Perez, R.; Pelletier, A.; Grenier, J.; Cros, J.; Rancourt, D.; Freer, R. Comparison between Space Mapping and Direct FEA Optimizations for the Design of Halbach Array PM Motor. *Energies* **2022**, *15*, 3969. [CrossRef]
24. Huang, C.; Kou, B.; Zhao, X.; Niu, X.; Zhang, L. Multi-Objective Optimization Design of a Stator Coreless Multidisc Axial Flux Permanent Magnet Motor. *Energies* **2022**, *15*, 4810. [CrossRef]
25. Abozar, A.; Ole-Morten, M. Winding loss analysis and optimization of an AC inductor for a galvanically isolated PV inverter. In Proceedings of the 2012 International Conference and Exposition on Electrical and Power Engineering, Iasi, Romania, 25–27 October 2012. [CrossRef]
26. Xi, N.; Sullivan, R.C. An improved calculation of proximity-effect loss in high-frequency windings of round conductors. In Proceedings of the IEEE 34th Annual Conference on Power Electronics Specialist, Acapulco, Mexico, 15–19 June 2003. [CrossRef]
27. Naoki, Y.; Kanako, S.; Makoto, S.; Toshiro, S. Fabrication and Evaluation of Composite Magnetic Core Using Iron-Based Amorphous Alloy Powder with Different Particle Size Distributions. *IEEE Trans. Magn.* **2018**, *54*, 1–5.
28. Prashant, S.; Pooja, S. Polymer Nanocomposites in Sensor Applications: A Review on Present Trends and Future Scope. *Chin. J. Polym. Sci.* **2021**, *39*, 665–691.
29. Hiremath, A.; Murthy, A.; Thipperudrappa, S.; Bharath, K.N. Nanoparticles Filled Polymer Nanocomposites: A Technological Review. *Cogent Eng.* **2021**, *8*, 1991229. [CrossRef]
30. Liu, Y.; Lu, Q.; Wang, J.; Zhao, X. A Flexible Sandwich Structure Carbon Fiber Cloth with Resin Coating Composite Improves Electromagnetic Wave Absorption Performance at Low Frequency. *Polymers* **2022**, *14*, 233. [CrossRef]
31. Bontas, M.G.; Diacon, A.; Calinescu, I.; Necolau, M.I.; Dinescu, A.; Toader, G.; Ginghina, R.; Viziriu, A.; Velicu, V.; Palade, P.; et al. Epoxy Coatings Containing Modified Graphene for Electromagnetic Shielding. *Polymers* **2022**, *14*, 2508. [CrossRef]
32. Chenggao, L.; Xiaoli, Y.; Yancong, L.; Rui, G.; Guo, X.; Guijun, X. Long-term service evaluation of a pultruded carbon/glass hybrid rod exposed to elevated temperature, hydraulic pressure and fatigue load coupling. *Int. J. Fatigue* **2020**, *134*, 105480.
33. Rui, G.; Guijun, X.; Feng, L.; Chenggao, L.; Bin, H. Hygrothermal resistance of pultruded carbon, glass and carbon/glass hybrid fiber reinforced epoxy composites. *Constr. Build. Mater.* **2022**, *315*, 125710.
34. Wang, B.; Li, D.; Xian, G.; Li, C. Effect of Immersion in Water or Alkali Solution on the Structures and Properties of Epoxy Resin. *Polymers* **2021**, *13*, 1902. [CrossRef]
35. Gimenez, R.; Serrano, B.; Miguel, V.S.; Cabanelas, J.C. Recent Advances in MXene/Epoxy Composites: Trend and Prospects. *Polymers* **2022**, *14*, 1170. [CrossRef]
36. Wu, J.; Li, C.; Hailatihan, B.; Mi, L.; Baheti, Y.; Yan, Y. Effect of the Addition of Thermoplastic Resin and Composite on Mechanical and Thermal Properties of Epoxy Resin. *Polymers* **2022**, *14*, 1087. [CrossRef]